Monitoring Wound Health through Bandages with Passive LC Resonant Sensors

Sadaf Charkhabi[1], Kyle J. Jackson[1], Andee M. Beierle[1], Adam R. Carr[1], Eric M. Zellner[2], Nigel F. Reuel[1*]

[1]Department of Chemical and Biological Engineering, Iowa State University, Ames, IA, 50011

[2]Department of Veterinary Clinical Sciences, Iowa State University, Ames, IA, 50011

* Corresponding Author – reuel@iastate.edu

Abstract

This paper details a passive, inductor-capacitor (LC) resonant sensor embedded in a commercial dressing for low-cost, contact-free monitoring of a wound; this would enable tracking of the healing process while keeping the site closed and sterile. Spiral LC resonators were fabricated from flexible, copper-coated polyimide and interrogated by external reader antennas connected to a two-port vector network analyzer (VNA); the forward transmission scattering parameter (S_{21}) magnitude was collected and the resonant frequency (MHz) and the peak-to-peak amplitude of the resonant feature were identified. These increase during the healing process as the permittivity and conductivity of the tissue change. The sensor was first tested on gelatin-based tissue mimicking phantoms (TMPs) that simulate layers of muscle, blood, fat, and skin at varying phases of wound healing. Finite element modeling was also used to verify the empirical results based on the expected variations in dielectric properties of the tissue. The performance of the resonant sensors for *in vivo* applications was investigated by conducting animal studies using canine patients that presented with natural wound as well as a controlled cohort of rat models with surgically administered wounds. Finally, transfer functions are presented that relate the resonant frequency to wound size using an exponential model (R^2 = 0.58 – 0.96). Next steps in sensor design and fabrication as well as the reading platform to achieve the goal of a universal calibration curve are then discussed.

Key Words: Resonant sensor| LC sensor| Wireless| Wound management| Smart bandage

The management of chronic skin wounds, especially pressure ulcers, diabetic foot ulcers, and surgical wounds, impose an immense economic burden (over US$25 billion in the US alone).[1] Worldwide, the upward trends in aging, obesity, and diabetes increase this burden.[2,3] Quality of life is affected as those with chronic wounds face more serious issues such as limb amputation and premature death caused by infection; therefore, regular and consistent wound monitoring is essential. [4] Wound assessment is most typically performed by physical inspection of the wound by trained, medical staff, which is not only less accurate, but also requires multiple trips to the hospital. Moreover, dressings need to be removed for visual wound inspection and this can impede the usual wound healing process in addition to causing increased pain and stress to the patient.[5] More advanced imaging methods have been developed in the past few decades for measuring the state of healing and diagnosis of a chronic wound such as measuring the wound volume using a plenoptic lens[6], hyperspectral imaging method for tissue oxygenation[7], and measuring the temperature profile of the wound area by infrared imaging.[8] The same disadvantages associated with wound dressing removal and costly hospital visits still apply to these enhanced imaging techniques. Hence, developing non-invasive, contact-free sensors that could be embedded into the wound dressing and report status without removal would be beneficial for reducing the pain, hospitalization time, frequency of dressing change, and overall healthcare cost.

Wireless sensors have been developed to monitor several markers of wound state such as temperature[9,10], moisture[11], pressure[12,13], pH[12,13], and oxygen.[14] For instance, an active (battery-powered) RFID tag coupled to a conducting film with temperature-dependent resistivity was developed to continuously monitor the local temperature of chronic wounds.[15] As a commercially available example, the WoundSense is a wearable wound moisture sensor, which works based on impedance measurement using a hand-held meter attached to the sensor, which has been applied to traumatic wound beds.[16] Multiple flexible sensors have been developed for continuous bandage pressure measurements, especially critical when using compression therapy.[5,17,18] A non-invasive flexible sensor array was developed for early detection of pressure ulcers using impedance spectroscopy across the flexible electrodes

attached to the wound.[19] Examples of pH monitoring for wounds include a textile-based design consisting of a pH-sensitive functional layer with gold wire electrodes connected to an impedance analyzer.[20] Oxygen concentration, which is an indicator of hypoxia in the chronic wound as well as angiogenesis rate, has been measured using a compact assembly of off-the-shelf, integrated electronics and a custom electrochemical galvanic cell coupled to real-time data acquisition and wireless transmission via Bluetooth.[21] However, distinguishing the oxygen level of the tissue from the oxygen of the air of the sensor surrounding environment is a confounding issue.[22] As an example of testing biomarkers, a screen-printed RFID tag was recently embedded in a wound dressing and connected to a potentiostat to measure and store the sensor current output which is correlated to the concentration of uric acid (UA); this is then wirelessly communicated with a smartphone.[23] The most important limitation of these existing approaches, is the need to include a local power source, which affects the price, durability, safety, and comfort of the wearable sensor. To overcome these challenges, passive LC sensors can also be employed for wound management, which enable continuous measurements without the need for internal battery, integrated memory chip, or wired connections.[24]

Inductor-capacitor (LC), resonant sensors are one class of passive devices that have shown promise for wound management. These sensors report changes in circuit inductance and capacitance, which can be tied to environmental changes[25,26] or specific, biological analytes.[27] They are interrogated via near-field coupling and do not have the need for an internal battery which makes them ideal for continuous monitoring of physical, chemical, and biological parameters in harsh environments as well as the human body.[24,28] These sensors have been applied to simulated tissue models, such as passive LC sensors embedded in tissue phantom models of malignant breast tissue.[29] LC sensors can also be coupled to a material sensitive to a wound marker. For instance, a passive LC sensor coupled to a poly(vinyl alcohol)–poly(acrylic acid) pH-responsive hydrogel was embedded in a wound dressing and transduced the pH of the wound liquid.[30] Pressure can also be sensed, such as study which used a passive wireless LC sensor having a microstructured, pyramidal, PDMS elastomer layer as the dielectric material embedded in a commercial bandage to track pressure change via resonant frequency

change.[31] Temperature can also be transduced using an LC sensor, such as one study presented using a porcine shank model to simulate orthopedic implant sites.[32] Finally, moisture level of the wound has been transduced with a flexible LC sensor using graphene oxide as the moisture sensitive material.[33] Although these works have shown great promise in applying resonant, LC sensors to contactless wound management in closed dressings, a major limitation has been demonstrating their utility on live animal models, especially those that are scanned over a longitudinal study. This is a key gap in literature, as LC sensors have significant positional dependence and must be studied in this context.[34] A moving animal is very different from a static tissue phantom or nonliving tissue model. Moreover, the basic mechanism of transducing changes in tissue dielectric and conductivity has not been explored.

Herein, we link the wound status response of LC sensors to changes in tissue dielectric using proxy tissue models[35], first-principle finite element simulations, and two living animal models (canine and murine). We use low-cost, passive Archimedean spiral resonant sensor patches embedded into a commercial wound dressing which wirelessly transduce the local tissue permittivity to an external reader antenna connected to a vector network analyzer (VNA). The magnitude of forward transmission scattering parameter (S_{21}) was collected at varying phases of wound healing. First, this was done with tissue mimicking phantoms (TMPs) that replicate the dielectric properties of muscle tissue, blood, fat, and skin.[36] These empirical findings were then corroborated with finite element modeling of the resonant sensor response to expected changes in tissue dielectric. Next, animal studies were conducted to determine the performance of the resonant sensors on a living, moving subject using one dog with an existing wound and a cohort of rats with surgically induced wounds. In the controlled rat study, the resonant frequency of the LC sensor was correlated to visual-based wound assessments.

This work presents a few novel advances to the existing body of LC work and passive wound sensors presented above. This is the first demonstration of applying a single-layer, LC sensor, which works based on self-capacitance for reporting the status of the wound area. This eliminates a smaller interdigital electrode region and increases the interrogation area as well as decreasing the sensor fabrication complexity. Also, the LC sensor response is directly tied to the changes in both permittivity and conductivity of the tissue, without using any secondary

parameter such as temperature, pressure, and pH. Additionally, a longitudinal study using LC sensor on animal models is presented for the first time, which calibrates the sensor response to the actual wound size extracted from image-based assessments. Discussion of the reliability and performance of these sensors is then presented along with next steps for further improvement.

Results and Discussion

Archimedean spiral resonators having an inner diameter of 1.5 mm, outer diameter of 40 mm, and pitch (sum of the conductive trace width and the line spacing) of 1.2 mm (resulting in 16 spiral turns) were fabricated by masking and chemical etching Pyralux as previously described.[27] The LC sensor and its substrate (polyimide) were covered with 3M Tegaderm, an FDA-approved, semi-permeable, commercially-available wound dressing, in order to insulate the conductive trace; this protects the sensor from shorting in the fluid-rich environment of the wound. The contact-free interrogation of the resonant sensor was then accomplished through electromagnetic, nearfield coupling to an external, two-loop, coplanar reader antenna, connected to a two-port vector network analyzer (VNA) (Figure 1a). A local electromagnetic field is generated when the reader antennas are excited by the VNA which leads to energy transfer to the proximal sensor. The VNA measures the forward transmission scattering parameter (S_{21}) of the coupled system (Figure 1b) which is recorded using custom MATLAB scripts (Supplement 1). The energy stored in the sensor from the first excited reader antenna loop (port 1) and the energy transferred from the sensor to the second receiver reader antenna loop (port 2) form a symmetric resonant feature with a peak and trough in the magnitude of S_{21}. We define the peak frequency of this feature as the sensor's resonant frequency, which is dependent on the sensor geometry as well as the effective permittivity of the sensor environment (Eq. 1). From the fundamental equation of resonant frequency (Eq. 1), we see that a decrease in permittivity or decrease in capacitance (C) would cause an increase in the resonant frequency. The difference in the magnitude of S_{21} for the peak and trough of the resonant feature is also defined as a sensor response (peak-to-peak amplitude), which is dependent on the effective resistance of the sensor and the conductivity of the sensor

surroundings. The resonant frequency and the peak-to-peak amplitude of the magnitude of S_{21} are determined using MATLAB scripts (Supplement 2).

$$f_{SR} = \frac{1}{2\pi\sqrt{LC}} \quad (1)$$

A preliminary animal study was conducted using copper-etched resonant sensor (Figure 1c-i) on a canine patient that presented with a large wound on top of its paw (Figure 1c-ii). The wound was covered with a 0.5 mm thick polyurethane foam pad and the sterilized resonant sensor patch (LC sensor covered with Tegaderm and autoclaved) was placed on the pad and then covered with multiple gauze layers (Figure 1c-iii). A similar patch was placed on a healthy tissue close to the wound area (also shaved portion of skin) and the magnitude of S_{21} was monitored for both resonators (Figure 1b). A detectable difference in the resonant frequency was observed between healthy and damaged tissue at each bandage change. Due to the changes in the wound area tissue during the wound healing/pathogenesis, the dielectric properties of the wound area changes over time.[29,37] Since the resonant sensor is sensitive to the relative permittivity of its environment, a shift in the resonant frequency can be observed if the LC sensor is in the proximity of the wound. The sensor placed on the healthy tissue resonates at higher frequency in comparison to the sensor placed on the wound area. This phenomenon can be attributed to higher levels of blood and wound exudates in the damaged tissue, which in general results in higher relative permittivity and lower resonant frequency. Furthermore, the damaged area has a smaller peak-to-peak amplitude in comparison to the normal skin due to the higher conductivity of blood which is present in the wound.[37]

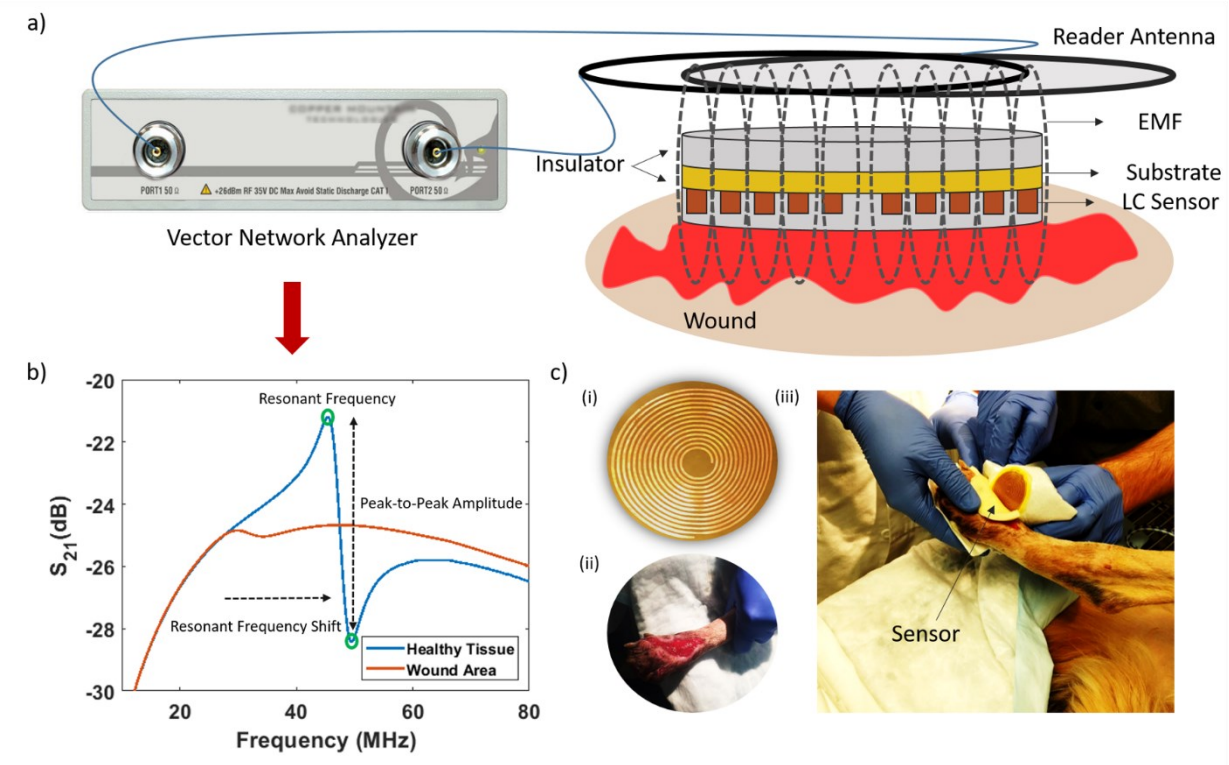

Figure 1. a) Side view schematic of resonant sensor system consisting of an LC sensor on a flexible substrate placed between two sterile insulator layers, and an external two-loop reader antenna connected to a two-port Vector Network Analyzer. The dotted ellipses represent the electromagnetic field which is influenced by the relative permittivity of the wound; b) Example of sensor transmission magnitude response when exposed to the healthy tissue and the wound area; the three extracted parameters are shown from the raw data c) Preliminary animal study using Archimedean resonant sensor (i) to monitor foot injury present on a dog patient (ii). The sensor response of the resonator placed in between wound bandage (iii) is shown in (b) compared to a second control sensor placed proximal to the wound, on healthy tissue.

In order to confirm the positive shift observed in the resonant frequency of these resonant sensors during the healing process of the wound, experiments were next conducted using tissue mimicking phantoms (TMPs) to simulate the different phases of wound healing (Fig 2a). TMPs are gelatin-based, proxy tissue structures that have been used for tissue dielectric spectroscopy, especially in evaluating the attenuation and absorptivity of electromagnetic fields from commercial devices such as cell phones[38] and medical imaging modalities (e.g. ultrasound, magnetic resonance imaging (MRI).[39,40] TMP recipes recreate tissue layers similar to wet skin, muscle, fat, and blood by varying the respective amounts of gelatin, water, oil, surfactant, and ions.[36,41] Layers of muscle, blood, fat, and skin TMPs were cast in a petri dish respectively and

then cavities with varying areas and depths were created and filled with blood proxy to represent different phases of wound healing in order to validate the applicability of resonant sensors to distinguish between the phases of healing (Figure 2b). A layer of Telfa, which is a specialized, sterile gauze pad that does not stick to the wound, was used as the primary layer of dressing and the resonant sensor was placed on top of the Telfa layer with its conductive trace facing towards the TMP. The resonant sensor was positioned so that the center of the spiral was aligned with the center of the wound. When monitoring the S_{21} signal, an increase in the resonant frequency was observed in the wound healing process (Figure 2c), which is in agreement with the preliminary canine study (Figure 1b). The shift in resonant frequency is attributed to the higher permittivity of blood phantom compared to the wet skin, fat, and muscle TMPs (Supplement 3).[36,42,43] In other words, at initial stages of wound healing, the blood phantom substitutes the muscle, fat, and wet skin layers, which result in a higher effective permittivity of the LC sensor and a lower resonant frequency. Moreover, the conductivity of the blood TMP is also higher than the muscle, wet skin, and fat TMPs, which results in smaller peak-to-peak amplitudes at early stages of the wound, which increases in the healing process (conductivity decreases).[36,42,43]

This positive shift in resonant frequency observed upon wound healing was then further assessed by simulating the resonant sensor on tissue layers simulated in finite element software (Ansys HFSS, Figure 2d). The simulated S_{21} signal is in fair agreement with the experimental results, showing both an increase in magnitude and resonant frequency when the resonant sensor is exposed to varying TMPs representing advanced stages of wound healing (Figure 2e).

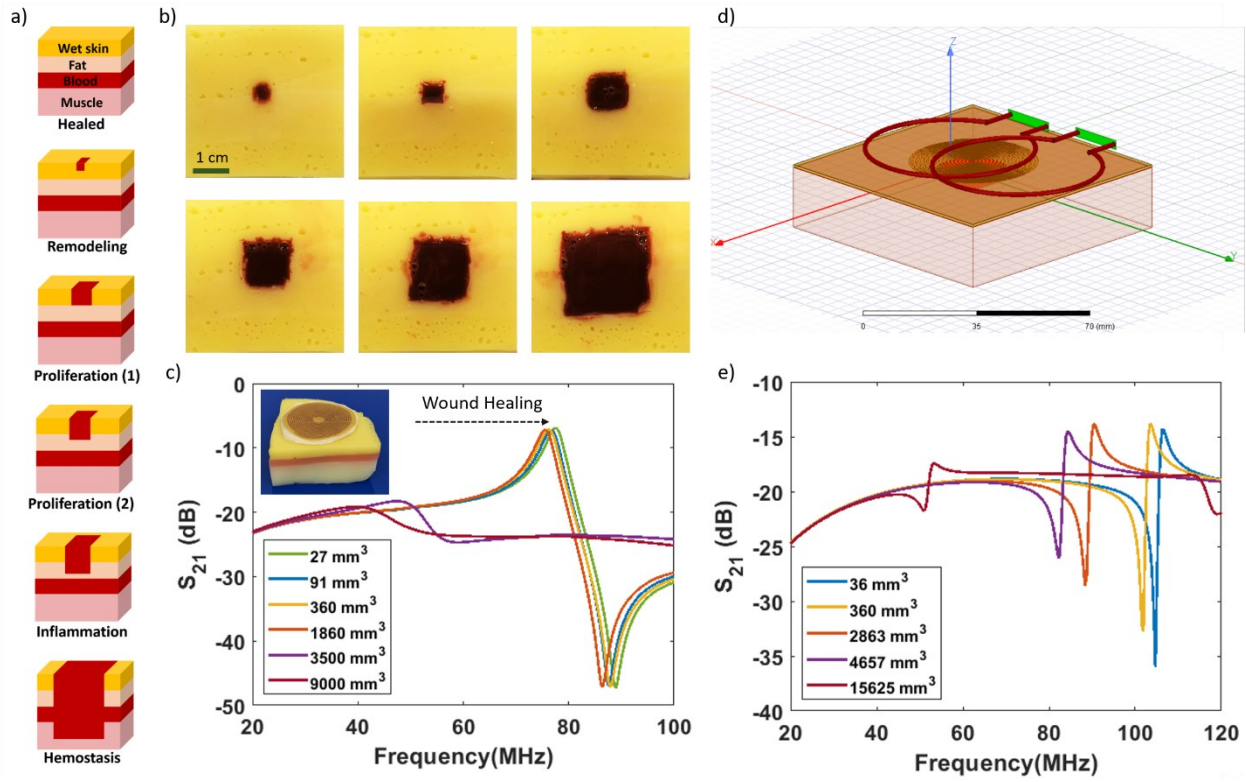

Figure 2. a) Cross-section drawing of various phases of wound healing that are then simulated with tissue mimicking phantoms (TMPs); b) Top view of TMPs consisting of muscle, blood, fat, and wet skin layers with various wound sizes; c) Sensor response to various stages of wound healing using TMPs (insert graph is the side view of resonant sensor on TMP). The arrow denotes the positive shift in the resonant frequency observed during the healing process; d) Angled view of TMP-sensor-reader setup for simulation; e) Simulated sensor response when exposed to different wound sizes.

Although the preliminary animal tests performed on natural wounds presented at the canine clinic point to practical use of resonant sensors to distinguish between the wound area and healthy tissue, there were not enough models or longitudinal study time to fully evaluate sensor performance. In order to evaluate the feasibility of using resonant sensors for longitudinal wound monitoring, a small cohort of 12 rats (Wistar, average weight ~ 270 g) (Figure 3a) were used, each with an administered wound of approximately 2 cm x 2 cm on their dorsal thorax (Supplement 4 for full rat specifications). We must emphasize that this initial sample size was large enough to only determine if there is a significant effect of healed tissue on the sensor in a longitudinal study; it is not large enough to establish a calibration curve nor reliability metrics; only after functionality is shown in this initial work would we want to

increase the number of animals needed to have such statistical power. We divided the cohort in an attempt to compare the healing rate of wounds treated with a conventional hydrogel (Covidien/Kendall amorphous hydrogel) to ones treated with vascular endothelial growth factor (VEGF). VEGF is a growth factor that assists in wound healing by developing new blood vessels that support granulation and tissue formation (*e.g.* promotes vasculogenesis and angiogenesis). In order to investigate the performance of VEGF compared to the conventional hydrogel, half of the rats were randomly selected and treated with 20 micrograms of VEGF per wound during each bandage change. The primary layer in contact with the wound was the treatment layer, which was either the hydrogel or VEGF. In order to investigate the effect of sensor displacement from the wound (a significant feature we observed with the TMPs) on acquiring a reliable, detectable response from the sensor, we placed Telfa in between the sensor and the treatment layer as a spacer for half of the rats. The sensor patch, consisting of the LC sensor on polyimide flexible substrate placed between Tegaderm (for insulation and sterility), was then attached to the rat using 3M Ioban (Figure 3b). Ioban is an antimicrobial adhesive which helps with both immobilizing the sensor on the rat as well as preventing wound contamination (Fig 3e).

The animal study began with surgically creating a 2 cm x 2 cm wound, removing the skin and the subcutaneous fat layer. The wound was then bandaged and monitored daily for the expected healing time (ranged from 12 to 42 days depending on the rat) via both visual inspection at bandage changes (not daily) and recording the scattering parameter response of the sensors via VNA excitation and signal analysis by MATLAB. For each measurement session, the rat was placed in a plastic sleeve (DecapiCone) to reduce movement and control changes caused by positional alignment; furthermore, the immobilized rat was carefully positioned in a cradle fixed to a lifting jack and the rat was then lifted up to 5 mm below the VNA antennas for each reading (Figure 3c). In addition to the sensor placed on the wound area, a second sensor was placed on the healthy, intact skin (control, also shaved) using the same bandage method in order to determine if the sensor response is significantly different when exposed to the wound area and healthy tissue (Figure 3d). The center of the spiral was marked and aligned with the center of the wound as well as the center of the coplanar reader to reduce variations in the

sensor response caused by positioning. As mentioned above, securing the resonant sensor with Ioban (Figure 3e) prevents sensor movement in between the measurement sessions which would lead to increased variability.

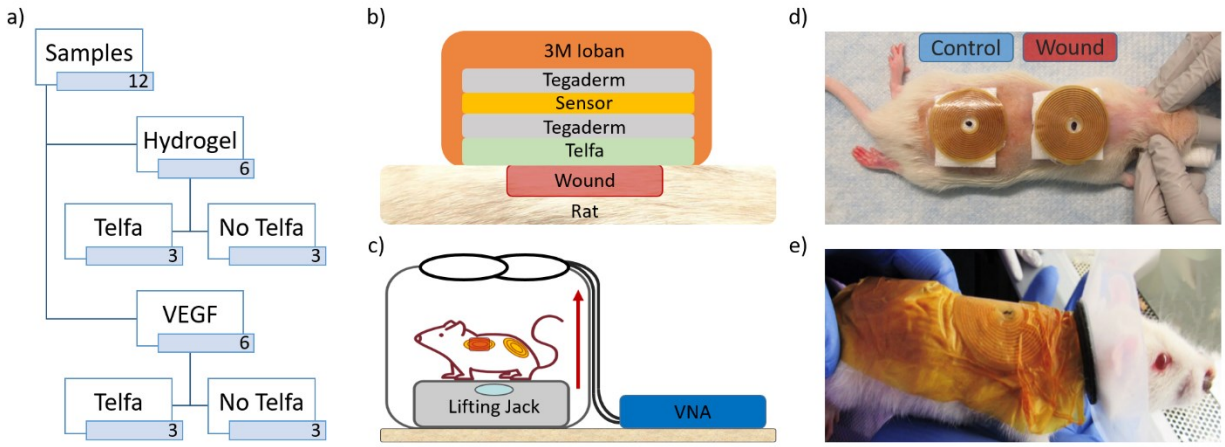

Figure 3. a) Rat study diagram showing different cohorts in the study; b) Side view schematic of layers used to attach the LC sensor on the rat; c) The reader setup used for measuring the scattering parameters of the sensors on the rat; d) Placement of sensor patches on the wound area and the healthy tissue on the back of the rat model; e) Securing sensor patches with 3M Ioban tape.

In addition to monitoring changes in the resonant sensor response, the wounds were visually assessed using conventional, image-based techniques when the wound dressing and the resonant sensors were changed every 2 to 3 days. Representative photographs from one of the models (Rat 907, which had a Telfa layer and was treated with VEGF) is shown (Figure 4a). The size of the wound and the average RGB color pixel intensity of the wound area were further analyzed (Figure 4b) using MATLAB scripts (Supplement 5). The wound size *vs.* time data is fit well with a decaying exponential function (R^2 = 0.95). Moreover, a reasonable linear correlation between the average color values of the R, G, and B channels *vs.* healing time was observed (R^2 = 0.48, 0.66, and 0.72 respectively). The low R^2 values obtained for the RGB model is attributed to variations in the light levels and photography angle in the vivarium.

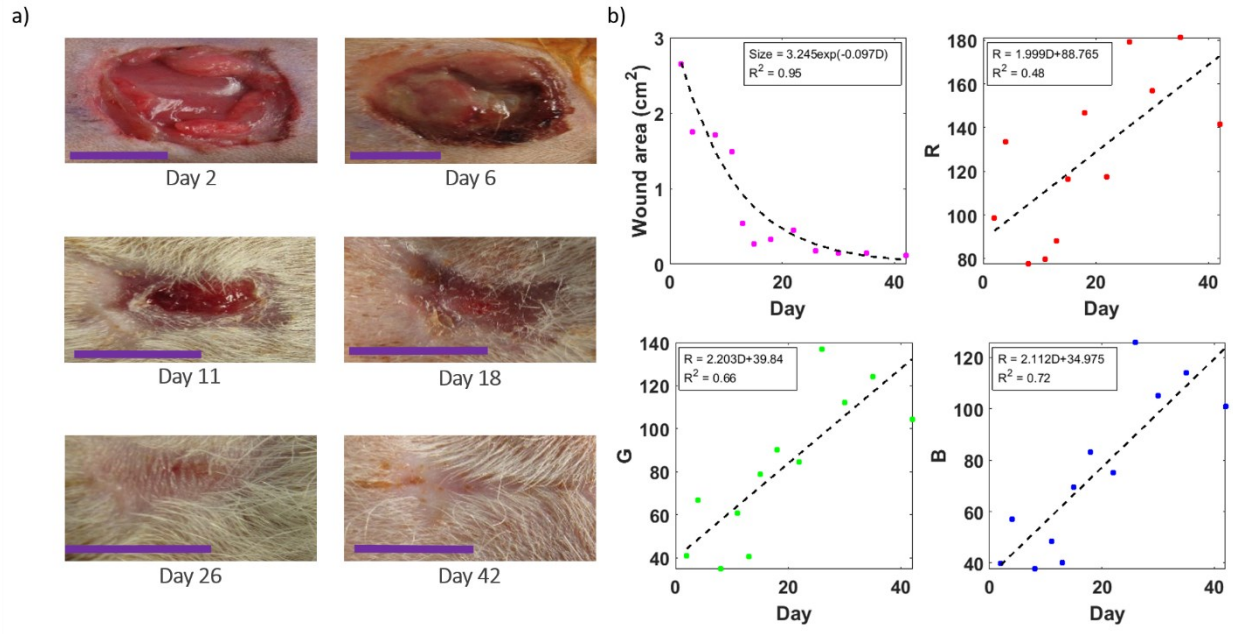

Figure 4. Image analysis of Rat 907, which was treated with VEGF and had a Telfa layer between the resonant sensor patch and the wound. a) Representative photograph of the wound at days 2, 6, 11, 18, 26, and 42 post-surgery (scale bar = 1 cm); b) Wound area and average RGB color pixel levels (Y scale max is 255 for 8 bit image) extracted from wound photographs using MATLAB.

Next the LC sensor data acquired over the wound healing phase were assessed. Example raw data of the LC sensor transmission magnitude response for the resonator placed on the healthy tissue (blue) and the wound area (orange) is demonstrated for rat 907 (Figure 5). In general, we observe that the resonant frequency and the peak-to-peak amplitude of the sensor placed on the normal intact skin remain fairly constant over the period of study; however, both of these measured parameters generally increase through the study time period for the sensor placed on the wound area. We attribute the increase in the resonant frequency to the decrease in the level of moisture content during the wound healing process. This would decrease the sensor self-capacitance and would thus increase the resonant frequency through the wound healing process (Eq. 1). The resonant frequency of the sensor placed on the healthy tissue is considerably lower during the first week of experiment due to the large load of blood and wound exudate at the early stages of healing, which also leaked to the healthy area (under the same large covering placed on the rat model).

Like the canine model and the tissue proxies, we observe that the peak-to-peak amplitude is larger at the later stages of healing. This is attributed to the peak-to-peak amplitude dependency on the conductivity of its surrounding environment and the free blood having a higher conductivity in comparison with skin, subcutaneous fat and the muscle tissue.[37] It is also important to note that the peak-to-peak amplitude is also strongly dependent on the displacement distance and angle between resonant sensor and reader.[34,44] We attempted to control these settings as much as possible with our reader setup (Fig 3c), but there is definitely more variance in these amplitude readings *vs.* frequency (which is less position and angle dependent).[34] Therefore, from this initial study we find that the resonant frequency is a more reliable measure of the sensor response.

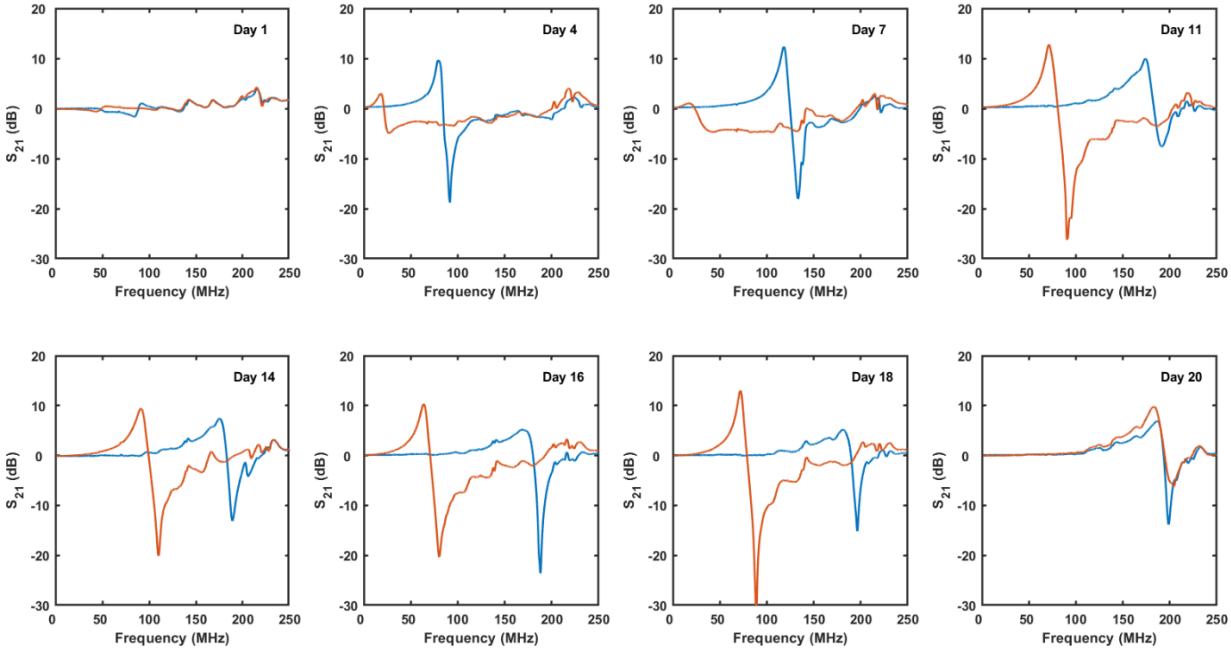

Figure 5. Example of S_{21} (dB) response of the resonant sensors placed on healthy tissue (blue) and wound area (orange) of Rat 907 at 1 to 20 days post-surgery.

As mentioned above, the rats were divided into four groups to study the effect of treatment methods on the wound healing as well as the effect of inserting a Telfa spacer on the quality of the S_{21} signal. The measured resonant frequencies and peak-to-peak amplitude for both sensors placed on the rats were tracked daily over the expected healing time. Due to the variations in the initial wound size, healing rate, and dressing layers across the animals,

analyzing the data of pooled animals as well as comparing the outcomes between the rats was inconsequent (Supplement 6). Thus we proceeded our analysis on an individual animal basis, comparing wound healing to their own internal control (the sensor on the healthy tissue). To first determine if there was a general shift between the healthy tissue sensor and wound sensor on each rat, all data was plotted as histograms and fit with lognormal or normal distributions based on goodness of fit (Fig 6 and 7). The rats for which a significant difference ($P<0.05$) between the distribution fit of the wound and control sensor response are noted. Based on this analysis, the presence of the Telfa layer was essential for better signal transduction (100% of the sensors with Telfa layer had significant difference between the healthy and healing tissue). This is likely due to direct contact of the sensor to wound exudate which shifts the resonant peak to below 1MHz and minimizes the peak to peak magnitude which makes it difficult to observe with our current reader. From the histograms, we also observe that the resonant frequency and peak-to-peak amplitude distributions of the sensors do not show a dependency on the method used for treating the wound (VEGF vs. hydrogel). However, VEGF slightly improved the wound healing rate, based on the visual inspections (Supplement 7). As discussed earlier, the resonant frequency is a better measure of the wound healing in comparison with peak-to-peak amplitude since the amplitude is impacted by the angle and the displacement between the reader and the sensor which we found challenging to completely prevent due to variations in the rat size and the curvature of the sensor placed on the rat.

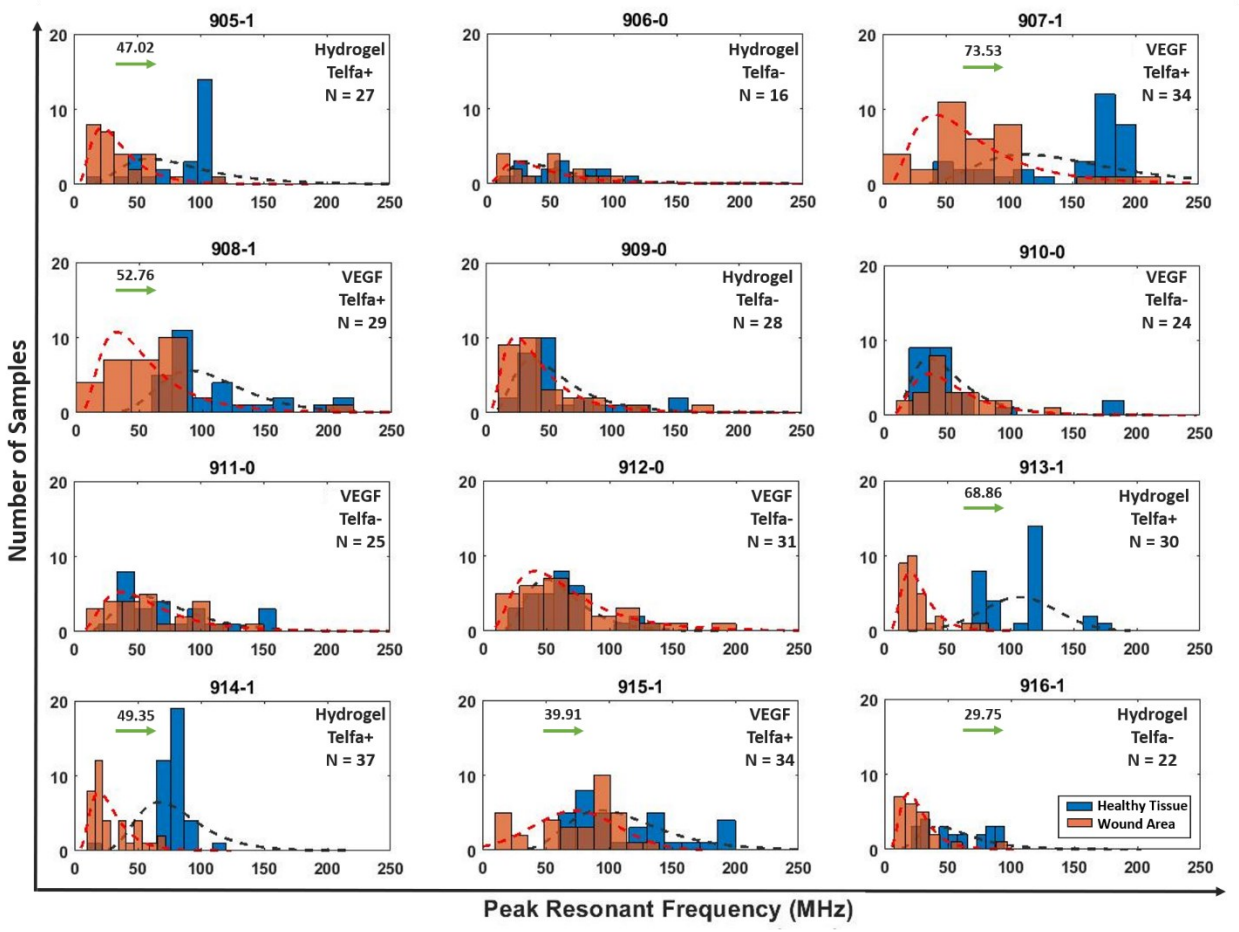

Figure 6. Histogram of sensor resonant frequency and the lognormal distribution fits for healthy tissue and wound area of all 12 rats. The "0" and "1" next to the rat number shows if there is no significant difference or significant difference between the resonant frequency of wound and healthy tissue, respectively. N represents the number of samples, which is equal to number of measurements taken during the longitudinal study for each rat. The x and y axes are peak resonant frequency and number of samples respectively (same for each sub-plot). The green arrow displays the positive shift in the resonant frequency of the rats for which the resonant frequency of the wound and healthy tissue were significantly different.

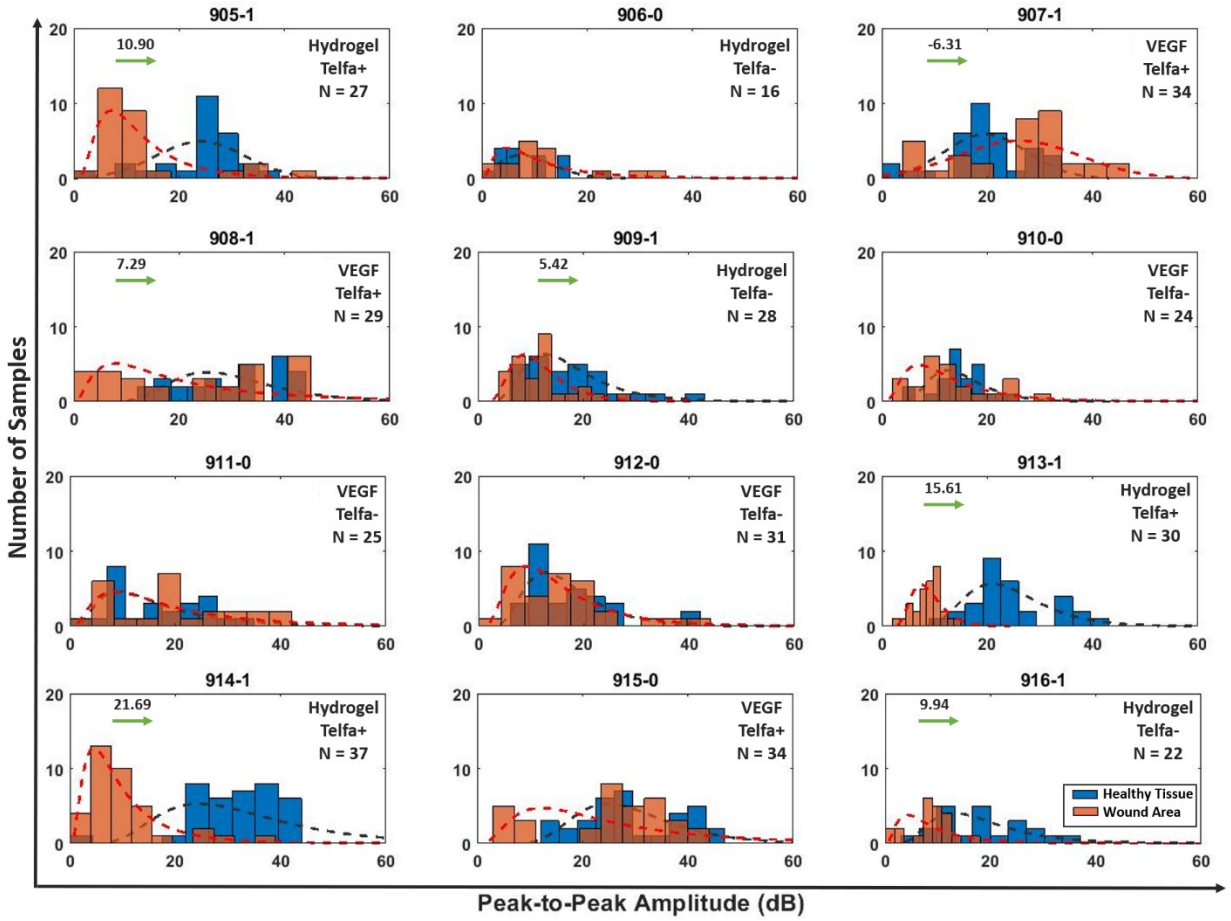

Figure 7. Histogram of sensor peak-to-peak amplitude and the lognormal distribution fits for healthy tissue and wound area of all 12 rats. The "0" and "1" next to the rat number shows if there is no significant difference or significant difference between the peak-to-peak amplitude of wound and healthy tissue, respectively. N represents the number of samples, which is equal to number of measurements taken during the longitudinal study for each rat. The x and y axes are peak to peak amplitude and number of samples respectively (same for each sub-plot). The green arrow displays the change in the peak-to-peak amplitude of the rats for which the peak-to-peak amplitude of the wound and healthy tissue were significantly different.

Based on the histogram data, three rats (VEGF: 907, 915 and Hydrogel: 914) with distinguishable resonant frequency shifts between wound area and healthy tissue were selected for further analysis of their longitudinal data. All sensors used on these rats were displaced from the tissue with a Telfa layer. Plotting the resonant frequency and peak-to-peak amplitude *vs.* time both show an increasing trend (Fig 8a and 9a respectively). The ultimate goal of this approach is to correlate the sensor response to actual wound size measured using a

conventional technique, such as imaging. The wound size measurements however, were only available for the days in which the bandage was changed; therefore, the daily wound area for each rat was estimated using the exponential model fit (Figure 4b). In general, the resonant frequency and the peak-to-peak amplitude are inversely related to the wound size (Figure 8b and Figure 9b, respectively). The resonant frequency *vs.* wound size data (Fig 8b) are fit well by exponential transfer functions (R^2 = 0.78 and 0.96). The hydrogel-treated rat had a longer healing time and its resonant frequency was fit, to less statistical significance, using a second order exponential decay function (R^2 = 0.58). Typical sensor parameters such as range, linearity, and sensitivity can be calculated for each rat (Supplement 8). For instance, the sensor has a linear response in the range of 30 – 65% wound closure for rat 915 with a sensitivity of 3.547 MHz/Wound closure%., which is fit well (R^2=0.94) using a linear function (Figure 8c). Although we were able to correlate the sensor resonant frequency to the wound size for each individual rat, we could not generate a single transfer function to be used as a global calibration curve for these sensors. This is attributed to the variabilities present in our study, such as variation in depth of the wound created for each rat, placement of the sensor on the wound each day, and small fabrication inconsistencies present. The peak-to-peak amplitude data (8b) exhibits a similar inverse trend, showing an increase in amplitude upon wound closure, but the noise of this measurement is much greater due to the proximity and placement effect which was difficult to control. However, both data sets point to the utility of this method and could be further improved upon implementing engineering strategies summarized below and by studying a larger cohort of rats.

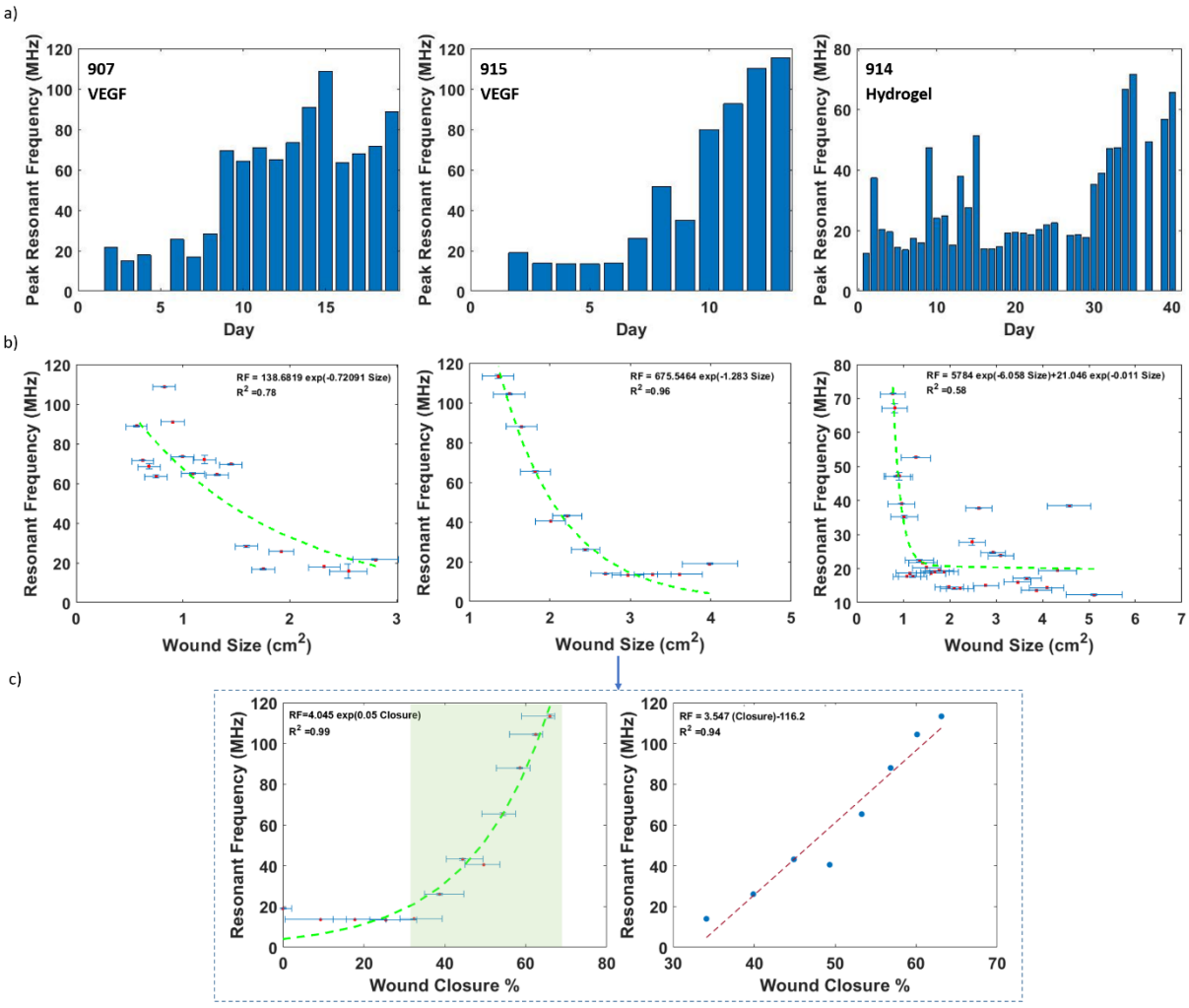

Figure 8. a) Measured resonant frequency; b) exponential model fits correlating the sensor resonant frequency to the visual wound area measurement for rats 907, 915, and 914; c) sensor resonant frequency response to wound closure in rat 915 and the linear region of the sensor response (depicted as green box). The X and Y error bars represent 68% confidence interval.

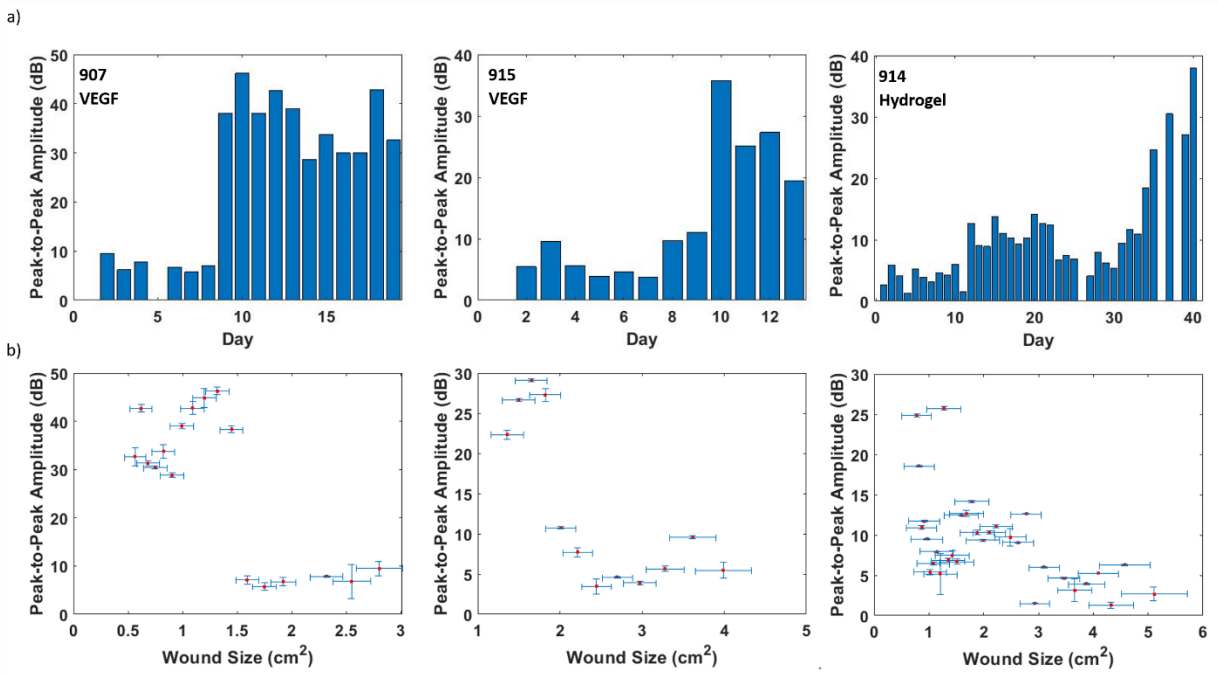

Figure 9. a) Measured peak-to-peak amplitude and b) correlation the sensor peak-to-peak amplitude to the visual wound area measurement for rats 907, 915, and 914. The X and Y error bars represent 68% confidence interval.

Conclusion

A flexible, passive LC sensor embedded in commercial wound dressing was investigated for wound monitoring applications. The decrease in relative permittivity of the tissue through the healing process causes an increase in the resonant frequency. Likewise, a decrease in wound fluid conductivity increases the peak to peak amplitude of the sensors. This response was observed using tissue mimicking phantoms, first-principle finite element simulations, one canine model with a natural wound and a cohort of 12 rats with surgically induced wounds. In these experiments, we found that having a sterile pad between the sensor and the wound was critical to improve the signal quality. Of the 6 rats that had the pad, three provided reliable enough data (reduced noise) to fit exponential transfer functions correlating the LC sensor response to wound size. However, these calibration curves were not consistent and varied in statistical significance. These could be further improved with experimental improvements detailed next. In this work, our sample size was too small (and the noise too great) to statistically show difference in wound treatment method (VEGF vs. hydrogel) using the LC sensor data; however, the traditional imaging approach showed a small improvement in wound

healing rate with VEGF and this could likely be transduced using an LC sensor with a larger animal cohort.

This first demonstration of LC sensors for wound healing in a controlled animal study revealed a few experimental changes that would improve sensor quality. First, the depth and size of the induced wounds should be better controlled, using a metal frame guide or other mechanical device to eliminate variability caused by free hand movement. Second, the reading platform can be improved to better position the rats or a hand-held portable VNA[34] could make the process of scanning the sensors more consistent. Including positional cues to correct alignment could also improve quality.[44] Third, designing resonant sensors with smaller features would reduce the curvature effect as well as enabling placement of more sensors at different locations of the wound on the same rat, thus improving our data set. Fourth, improving resonant sensor fabrication consistency by substituting chemical-etching technique with screen printing method would help with the uniformity of resonant sensors dielectric properties. Finally, with these new design strategies in place, the study could be further improved by increasing the number of subjects in the study. A larger cohort of animals would enable conducting control experiments (no sensor placed on the wound area) in order to determine if the presence of the sensor delays the wound healing process.

With further refinement, the resonant LC sensors introduced here could be used for frequent, at-home wound assessment. It is important to note, that if a universal calibration curve is not found, this method could still have utility in augmenting healing measurements between clinic visits; the clinically measured points would be used to map the LC response to actual measurement on a patient to patient basis. This could be of especial use in telemedicine situations where visits to the clinic may be less frequent. Moreover, this would have a significant impact in improving wound management by eliminating the need for unnecessary bandage changes for visual wound inspection as well as the associated cost of such clinic visits.

Experimental Section

Sensor fabrication. Archimedean spirals with dimensions of 1.5 mm inner diameter, 40 mm outer diameter, and 1.2 mm pitch size were designed in CAD software (Rhinoceros 5). The

spiral was then masked on the copper side of DuPont Pyralux, which is a single-sided, copper-clad polyimide, using an x–y plotter (Curio printer). The samples were then submerged in an etchant solution consisting of a 2:1 ratio solution of 3 wt% hydrogen peroxide (Carolina Biological) and 31.45 wt% hydrochloric acid (Fisher Scientific) for 10 to 15 minutes to remove the unmasked copper. The spiral mask was then released using acetone.

Signal Acquisition. The magnitude of forward scattering parameter signal (S_{21} (dB)) was measured using a two-loop coplanar external reader antenna which was placed in close proximity of the resonant sensor. The reader antenna loops, with 54 mm diameter each, were set in a 3D-printed reader frame with an overlap of 26.7 mm. The center of this overlap was perforated to be aligned with the center of the spiral resonator. The reader antenna was connected to a two-port VNA (TR1300/1 2-Port 1.3 GHz Analyzer, Copper Mountain Technologies). In the frequency range of 0 – 250 MHz, the phase and the magnitude of S_{21} and S_{11} were recorded using an automated MATLAB script. In order to calculate the resonant frequency and the peak-to-peak amplitude, the magnitude of S_{21} signal was further analyzed and the frequency and the magnitude of the peak and trough of the resonant features were extracted using another custom MATLAB script (Supplement 2).

Canine animal study. The *in vivo* performance of resonant sensors was initially evaluated using dogs that presented with natural injuries at Iowa State University Small Animal Hospital, Ames, Iowa (under IACUC-18-242, owner consented to testing of sensor). The resonant sensors were autoclaved for sterilization purposes and then insulated with sterile, 3M Tegaderm. After cleaning and covering the wound with a 0.5 mm polyurethane foam pad, the sensor patch was placed on the pad and was further covered with multiple layers of cast padding and CoFlex flexible cohesive bandage. A second sensor patch was placed on the shaved normal skin in proximity to the damaged area and then covered with similar bandage thicknesses (approximately 1 cm). The center of the resonators were marked on the outer bandage layer to reduce the variations caused by sensor-reader positioning. Both sensors were scanned externally by placing a two-loop reader antenna affixed to a handheld vector network analyzer (purchased from Metrovna Deluxe) on the bandage so that the center of the reader antenna is aligned with the center of the resonator.

Tissue mimicking phantoms preparation. Muscle, blood, fat, and wet skin tissue mimicking phantoms (TMPs) were made using the recipe provided by Yilmaz *et. al* (Supplement 9).[36] For each layer, the fabrication started with mixing 100 g deionized water and gelatin (Carolina Biological) in a covered beaker placed on a ceramic stirring hot plate (Thermo Scientific). The mixture was heated to 80°C and then cooled to 35°C, while stirring. The remaining deionized water as well as the NaCl were added to the mixture. The oil, detergent, and food coloring were added to the mixture when it reached 28°C; when the mixture became homogenous, it was poured in the mold. The phantom was made layer by layer, after each previous layer was solidified in the mold to prevent mixing of the layers. The thickness of muscle, blood, and wet skin layers were 15, 2.5, 2 mm, respectively. The fat tissue proxy was rubbed on the blood layer since it did not form a gel using the published recipe. Cavities with varying area and depth (Supplement 9) replicating various stages of the wound were created and then filled with the extra blood phantom, which was kept in liquid form on the hot plate. The wound area was covered with Telfa and the sensor patch was placed on top of this primary layer so that its conductive trace was facing towards the TMP and the spiral center was aligned with the center of the wound. The reader antenna was fixed at 5mm above the sensor for recording the S_{21} signal.

Rat animal study. Under IACUC-19-246, A cohort of 12 Wistar line rats with average weight of ~ 270 g were premedicated with midazolam (2 mg/kg) and buprenorphine (0.03 mg/kg) intramuscular (IM) and placed on isoflurane and oxygen via mask. A wound with approximate dimension of 2 cm x 2 cm was surgically created on their dorsal thorax by removing the skin and the subcutaneous fat excised to the muscle/fascial layer. An intact area of skin close to the wound was also shaved for the control resonator. The rats were randomly divided into two treatment groups of VEGF or hydrogel (20 micrograms per wound per bandage change). Within each treatment group, three rats were randomly selected for placement of a Telfa layer in between the wound/normal skin and the sensor patch (LC sensor on polyimide substrate placed between Tegaderm). The sensor patches were placed over the wound and intact skin, followed by 3M Ioban. At early stages of the wound, cast padding and vetwrap were also used for further immobilization. The resonators were scanned daily in order to record the

scattering parameter response and the visual inspection was conducted during the bandage change (every 2 – 5 days) over the wound healing period, which ranged from 12 – 42 days for rats in this study.

For the visual inspection, after removing the sensor and lavaging the wound, a photograph of the wound area was taken using a Canon Powershot SX530 camera. The wound size and the average RGB color pixel intensity (in the range of 0 – 255) was then calculated using custom MATLAB script (supplement 5). The setup used for scanning the resonators consisted of a semicircle frame (rat holder) fixed on a lifting jack inside an acrylic box. The two-loop reader was secured on the top surface of the box and was connected to the Copper Mountain TR1300/1 2-Port 1.3 GHz vector network analyzer via RF-shielded BNC cables. The cables were also fixed in position to eliminate additional signal noise. In order to record the scattering parameter signal, the rat was placed in a plastic sleeve (DecapiCone) and positioned on the lifting jack frame. The rat was then lifted up so that the distance between the sensor and the reader was approximately 5 mm and the center of the sensor and the reader were aligned. The raw scattering parameters of both resonators on damaged and normal skin were recorded over 0 – 250 MHz frequency range using MATLAB scripts. The data was then post-processed to determine resonant frequency and the peak-to-peak amplitude.

Supporting Information

The Supporting Information is available free of charge:

MATLAB code for recording scattering parameters and detecting the resonance feature, dielectric properties of various tissue types, rat animal study specification, wound visual assessment, sensor response comparison between the rats, effect of treatment method on wound healing rate, and TMP recipe and cavity size.

Acknowledgments

This study was partially supported by an NSF Industrial Innovation and Partnerships PFI-RP grant under award #1827578, NSF I-Corps grant under award #1924882, and a 3M Untenured Faculty Award to NFR.

References

(1) Järbrink, K.; Ni, G.; Sönnergren, H.; Schmidtchen, A.; Pang, C.; Bajpai, R.; Car, J. The Humanistic and Economic Burden of Chronic Wounds : A Protocol for a Systematic Review. *Syst. Rev.* **2017**, 1–7.

(2) Brem, H.; Stojadinovic, O.; Diegelmann, R. F.; Entero, H.; Lee, B.; Pastar, I.; Golinko, M.; Rosenberg, H.; Tomic-Canic, M. Molecular Markers in Patients with Chronic Wounds to Guide Surgical Debridement. *Mol. Med.* **2007**, *13* (1), 30–39.

(3) Sen, C. K.; Gordillo, G. M.; Roy, S.; Kirsner, R.; Lambert, L.; Hunt, T. K.; Gottrup, F.; Gurtner, G. C.; Longaker, M. T. Health and the Economy. **2010**, *17* (6), 763–771.

(4) Gottrup, F.; Sci, D. M. A Specialized Wound-Healing Center Concept : Importance of a Multidisciplinary Department Structure and Surgical Treatment Facilities in the Treatment of Chronic Wounds. **2004**, *187* (May), 19–20.

(5) Mehmood, N.; Hariz, A.; Fitridge, R.; Voelcker, N. H. Applications of Modern Sensors and Wireless Technology in Effective Wound Management. *J. Biomed. Mater. Res. Part B Appl. Biomater.* **2014**, *102* (4), 885–895.

(6) Shademan, A.; Decker, R. S.; Opfermann, J.; Leonard, S.; Kim, P. C. W.; Krieger, A. Plenoptic Cameras in Surgical Robotics: Calibration, Registration, and Evaluation. In *2016 IEEE International Conference on Robotics and Automation (ICRA)*; IEEE, 2016; pp 708–714.

(7) Kuppusamy, P.; Chzhan, M.; Vij, K.; Shteynbuk, M.; Lefer, D. J.; Giannella, E.; Zweier, J. L. Three-Dimensional Spectral-Spatial EPR Imaging of Free Radicals in the Heart: A Technique for Imaging Tissue Metabolism and Oxygenation. *Proc. Natl. Acad. Sci.* **1994**,

91 (8), 3388–3392.

(8) Paul, D. W.; Ghassemi, P.; Ramella-Roman, J. C.; Prindeze, N. J.; Moffatt, L. T.; Alkhalil, A.; Shupp, J. W. Noninvasive Imaging Technologies for Cutaneous Wound Assessment: A Review. *Wound Repair Regen.* **2015**, *23* (2), 149–162.

(9) Armstrong, D. G.; Holtz-Neiderer, K.; Wendel, C.; Mohler, M. J.; Kimbriel, H. R.; Lavery, L. A. Skin Temperature Monitoring Reduces the Risk for Diabetic Foot Ulceration in High-Risk Patients. *Am. J. Med.* **2007**, *120* (12), 1042–1046.

(10) Nakagami, G.; Sanada, H.; Iizaka, S.; Kadono, T.; Higashino, T.; Koyanagi, H.; Haga, N. Predicting Delayed Pressure Ulcer Healing Using Thermography: A Prospective Cohort Study. *J. Wound Care* **2010**, *19* (11), 465–472.

(11) McColl, D.; Cartlidge, B.; Connolly, P. Real-Time Monitoring of Moisture Levels in Wound Dressings in Vitro: An Experimental Study. *Int. J. Surg.* **2007**, *5* (5), 316–322.

(12) Keller, A.; Müller, M. L.; Calow, T.; Kern, I. K.; Schumann, H. Bandage Pressure Measurement and Training: Simple Interventions to Improve Efficacy in Compression Bandaging. *Int. Wound J.* **2009**, *6* (5), 324–330.

(13) Wong, I. K. Y.; Andriessen, A.; Lee, D. T. F.; Thompson, D.; Wong, L. Y.; Chao, D. V. K.; So, W. K. W.; Abel, M. RETRACTED: Randomized Controlled Trial Comparing Treatment Outcome of Two Compression Bandaging Systems and Standard Care without Compression in Patients with Venous Leg Ulcers. Elsevier 2012.

(14) Sen, C. K. Wound Healing Essentials: Let There Be Oxygen. *Wound repair Regen.* **2009**, *17* (1), 1–18.

(15) Matzeu, G.; Losacco, M.; Parducci, E.; Pucci, A.; Dini, V.; Romanelli, M.; Di Francesco, F. Skin Temperature Monitoring by a Wireless Sensor. In *IECON 2011-37th Annual Conference of the IEEE Industrial Electronics Society*; IEEE, 2011; pp 3533–3535.

(16) Milne, S. D.; Seoudi, I.; Al Hamad, H.; Talal, T. K.; Anoop, A. A.; Allahverdi, N.; Zakaria, Z.; Menzies, R.; Connolly, P. A Wearable Wound Moisture Sensor as an Indicator for Wound

Dressing Change: An Observational Study of Wound Moisture and Status. *Int. Wound J.* **2016**, *13* (6), 1309–1314.

(17) Cheng, M.-Y.; Tsao, C.-M.; Lai, Y.-Z.; Yang, Y.-J. The Development of a Highly Twistable Tactile Sensing Array with Stretchable Helical Electrodes. *Sensors Actuators A Phys.* **2011**, *166* (2), 226–233.

(18) Ochoa, M.; Rahimi, R.; Ziaie, B. Flexible Sensors for Chronic Wound Management. *IEEE Rev. Biomed. Eng.* **2013**, *7*, 73–86.

(19) Swisher, S. L.; Lin, M. C.; Liao, A.; Leeflang, E. J.; Khan, Y.; Pavinatto, F. J.; Mann, K.; Naujokas, A.; Young, D.; Roy, S. Impedance Sensing Device Enables Early Detection of Pressure Ulcers in Vivo. *Nat. Commun.* **2015**, *6*, 6575.

(20) Nocke, A.; Schröter, A.; Cherif, C.; Gerlach, G. Miniaturized Textile-Based Multi-Layer Ph-Sensor for Wound Monitoring Applications. *Autex Res. J.* **2012**, *12* (1), 20–22.

(21) Mostafalu, P.; Lenk, W.; Dokmeci, M. R.; Ziaie, B.; Khademhosseini, A.; Sonkusale, S. R. Wireless Flexible Smart Bandage for Continuous Monitoring of Wound Oxygenation. *IEEE Trans. Biomed. Circuits Syst.* **2015**, *9* (5), 670–677.

(22) Derakhshandeh, H.; Kashaf, S. S.; Aghabaglou, F.; Ghanavati, I. O.; Tamayol, A. Smart Bandages: The Future of Wound Care. *Trends Biotechnol.* **2018**, *36* (12), 1259–1274.

(23) Kassal, P.; Kim, J.; Kumar, R.; de Araujo, W. R.; Steinberg, I. M.; Steinberg, M. D.; Wang, J. Smart Bandage with Wireless Connectivity for Uric Acid Biosensing as an Indicator of Wound Status. *Electrochem. commun.* **2015**, *56*, 6–10.

(24) Li, C.; Tan, Q.; Jia, P.; Zhang, W.; Liu, J.; Xue, C.; Xiong, J. Review of Research Status and Development Trends of Wireless Passive Lc Resonant Sensors for Harsh Environments. *Sensors (Switzerland)* **2015**, *15* (6), 13097–13109.

(25) Ong, K. G.; Grimes, C. A.; Robbins, C. L.; Singh, R. S. Design and Application of a Wireless, Passive, Resonant-Circuit Environmental Monitoring Sensor. *Sensors Actuators A Phys.* **2001**, *93* (1), 33–43.

(26) Charkhabi, S.; Chan, Y. J.; Hwang, D.; Frey, S. T.; Bartlett, M. D.; Reuel, N. F. Kirigami-Enabled, Passive Resonant Sensors for Wireless Deformation Monitoring. *Adv. Mater. Technol.* **2019**.

(27) Charkhabi, S.; Beierle, A.; McDaniel, M. D.; Reuel, N. F. Resonant Sensors for Low-Cost, Contact-Free Measurement of Hydrolytic Enzyme Activity in Closed Systems. *ACS Sensors* **2018**.

(28) Huang, Q. A.; Dong, L.; Wang, L. F. *LC Passive Wireless Sensors Toward a Wireless Sensing Platform: Status, Prospects, and Challenges*; 2016; Vol. 25, pp 822–841.

(29) Yvanoff, M. LC Sensor for Biological Tissue Characterization. **2008**.

(30) Sridhar, V.; Takahata, K. A Hydrogel-Based Passive Wireless Sensor Using a Flex-Circuit Inductive Transducer. *Sensors Actuators A Phys.* **2009**, *155* (1), 58–65.

(31) Deng, W.-J.; Wang, L.-F.; Dong, L.; Huang, Q.-A. LC Wireless Sensitive Pressure Sensors with Microstructured PDMS Dielectric Layers for Wound Monitoring. *IEEE Sens. J.* **2018**, *18* (12), 4886–4892.

(32) Karipott, S. S.; Veetil, P. M.; Nelson, B. D.; Guldberg, R. E.; Ong, K. G. An Embedded Wireless Temperature Sensor for Orthopedic Implants. *IEEE Sens. J.* **2017**, *18* (3), 1265–1272.

(33) Deng, W.-J.; Wang, L.-F.; Dong, L.; Huang, Q.-A. Flexible Passive Wireless Pressure and Moisture Dual-Parameter Sensor for Wound Monitoring. In *2018 IEEE SENSORS*; IEEE, 2018; pp 1–4.

(34) Carr, A. R.; Patel, Y. H.; Neff, C. R.; Charkhabi, S.; Kallmyer, N. E.; Angus, H. F.; Reuel, N. F. Sweat Monitoring beneath Garments Using Passive, Wireless Resonant Sensors Interfaced with Laser-Ablated Microfluidics. *npj Digit. Med.* **2020**, *3* (1), 1–9.

(35) Reuel, N. F.; Charkhabi, S. Wireless Tissue Dielectric Spectroscopy with Resonant Sensors. 16/667,671, **2020**.

(36) Yilmaz, T.; Member, S.; Foster, R.; Hao, Y. Broadband Tissue Mimicking Phantoms and a

Patch Resonator for Evaluating Noninvasive Monitoring of Blood Glucose Levels. *IEEE Trans. Antennas Propag.* **2014**, *62* (6), 3064–3075.

(37) Hasgall, P. A.; Neufeld, E.; Gosselin, M. C.; Klingenböck, A.; Kuster, N.; Hasgall, P.; Gosselin, M. IT'IS Database for Thermal and Electromagnetic Parameters of Biological Tissues. **2012**.

(38) Lazebnik, M.; Madsen, E. L.; Frank, G. R.; Hagness, S. C. Tissue-Mimicking Phantom Materials for Narrowband and Ultrawideband Microwave Applications. *Phys. Med. Biol.* **2005**, *50* (18), 4245.

(39) Choi, M. J.; Guntur, S. R.; Lee, K. I. L.; Paeng, D. G.; Coleman, A. A Tissue Mimicking Polyacrylamide Hydrogel Phantom for Visualizing Thermal Lesions Generated by High Intensity Focused Ultrasound. *Ultrasound Med. Biol.* **2013**, *39* (3), 439–448.

(40) Yuan, Y.; Wyatt, C.; Maccarini, P.; Stauffer, P.; Craciunescu, O.; MacFall, J.; Dewhirst, M.; Das, S. K. A Heterogeneous Human Tissue Mimicking Phantom for RF Heating and MRI Thermal Monitoring Verification. *Phys. Med. Biol.* **2012**, *57* (7), 2021.

(41) Dabbagh, A.; Abdullah, B. J. J.; Ramasindarum, C.; Abu Kasim, N. H. Tissue-Mimicking Gel Phantoms for Thermal Therapy Studies. *Ultrason. Imaging* **2014**, *36* (4), 291–316.

(42) Gabriel, S.; Lau, R. W.; Gabriel, C. The Dielectric Properties of Biological Tissues: II. Measurements in the Frequency Range 10 Hz to 20 GHz. *Phys. Med. Biol.* **1996**, *41* (11), 2251.

(43) Gabriel, S.; Lau, R. W.; Gabriel, C. The Dielectric Properties of Biological Tissues: III. Parametric Models for the Dielectric Spectrum of Tissues. *Phys. Med. Biol.* **1996**, *41* (11), 2271.

(44) Chan, Y. J.; Carr, A. R.; Charkhabi, S.; Furnish, M.; Beierle, A. M.; Reuel, N. F. Wireless Position Sensing and Normalization of Embedded Resonant Sensors Using a Resonator Array. *Sensors Actuators A Phys.* **2020**, *303*, 111853.

For TOC Only:

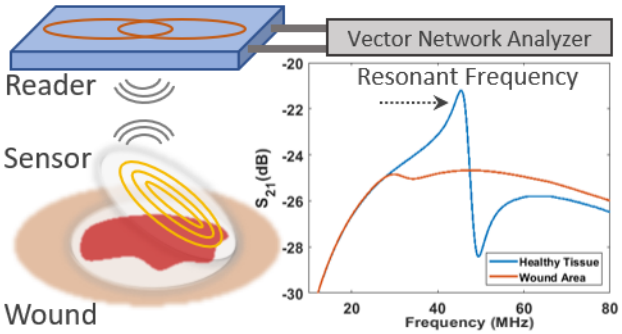
Vector Network Analyzer
Reader
Sensor
Wound
Resonant Frequency
S_{21}(dB)
-20
-22
-24
-26
-28
-30
20
40
60
80
Frequency (MHz)
Healthy Tissue
Wound Area